Journal of Materials Chemistry A

PAPER

View Article Online
View Journal | View Issue

Cite this: J. Mater. Chem. A, 2019, 7, 18397

Gas transport regulation in a MO/MOF interface for enhanced selective gas detection†

Ming-Shui Yao,‡[a] Lin-An Cao,‡[ac] Yong-Xiang Tang,[b] Guan-E. Wang,[a] Rui-Heng Liu,[a] P. Naresh Kumar,[a] Guo-Dong Wu,[a] Wei-Hua Deng,[a] Wen-Jing Hong *[b] and Gang Xu *[ac]

Received 17th May 2019
Accepted 6th July 2019

DOI: 10.1039/c9ta05226g

rsc.li/materials-a

The important application of metal oxides (MOs) as a chemiresistive sensing material can be severely hampered by their poor selectivity towards analyte molecules that possess a similar sensing activity. In this work, a new metal oxide@metal–organic framework (MO@MOF) core–sheath nanowire array material was prepared. Using a post-synthetic modification of the pore size in the MOF sheath, the channel traffic of the analyte molecules with a similar sensing activity but different kinetic diameter was successfully modulated, which profoundly enhanced the selectivity of the MOs. As a result, the materials obtained showed the highest selective response to acetone in the presence of benzene in all the reported materials.

Introduction

Chemiresistive gas sensors have great potential for use in applications in environment monitoring, intelligent traffic systems, disease diagnosis, public security, the food industry, and so on[1–5] Metal oxides (MOs, also represented as MOXs or MOxs) are one of the dominant materials used in chemiresistive sensors, however, they are significantly limited in their applications by their poor selectivity.[1,3,6,7] Methods such as lattice/new phase doping, heterojunctions, hybridization with catalysts, and functionalization with sensing probes, have been developed to enhance their selectivity towards molecules with significant differences in redox activity or specific interactions with MOs.[2,7–10] However, developing a material design strategy for MOs to further enhance their selectivity towards molecules that possess a similar sensing activity, (*e.g.*, acetone and the benzene series of compounds) is still a big challenge.

Metal–organic frameworks (MOFs) or porous coordination polymers are types of microporous crystalline materials.[11–26] The pore structure of MOFs can be flexibly modified to control the channel traffic to achieve selective gas/vapor separation.[27–34] The MOFs and MOF-derived materials have shown promising applications as advanced materials by their direct usage or compositing them with other materials, which possess advantageous features such as high surface areas, ordered multilevel porosities, and designable functionalities.[9,14,35–46] Previous reports by other groups and ours indicate that constructing a MO@MOF core–sheath/shell nanostructure is an ideal material design strategy to combine the high sensitivity of MO and the high selectivity of MOFs together to diminish the barriers for gas sensors. It was noted that the kinetic diameters (D_k) of the analyzed molecules with similar sensing activities are different. This provides the possibility to improve the selectivity of the MO core by modulating the channel traffic of the analyzed molecules in the MOF sheath by the difference in their D_k. However, it is still challenging to control the growth of a continuous MOF thin film on the surfaces of chemiresistive MO sensing materials. In the limited successful cases, the MOF sheaths, such as zeolitic imidazolate framework −8[ZIF-8(Zn-2-MIM, where 2-MIM = 2-methylimidazole)], and MIL-125,[11,14,29] have drawbacks of dynamically open and/or oversized apertures, which fails in controlling the traffic of molecules with similar sensing activities.

In this paper, it is reported that the selectivity of MOs towards molecules with a similar sensing activity, has been significantly enhanced by controlling the channel traffic of these molecules in the MOF sheath. As a proof-of-concept, a new MO@MOF core–sheath NWA material, gold–zinc oxide (Au–ZnO)@ZIF-8-DMBIM (DMBIM = 5,6-dimethylbenzimidazole, a hydrophobic ligand with a larger size than 2-MIM) with a narrower aperture size and better anti-humidity properties than Au–ZnO@ZIF-8 was prepared.[47,48] The traffic control of acetone and benzene series chemicals was realized by using an *in situ* post-synthetic modification, shell-ligand-exchange-

[a]State Key Laboratory of Structural Chemistry, Fujian Institute of Research on the Structure of Matter, Chinese Academy of Sciences (CAS), 155 Yangqiao Road West, Fuzhou, Fujian, 350002 P. R. China. E-mail: gxu@fjirsm.ac.cn

[b]College of Chemistry and Chemical Engineering, Xiamen University, 422 Siming South Road, Xiamen 361005, P. R. China. E-mail: whong@xmu.edu.cn

[c]University of Chinese Academy of Sciences (UCAS), No. 19A Yuquan Road, Beijing 100049, P. R. China

† Electronic supplementary information (ESI) available. See DOI: 10.1039/c9ta05226g

‡ These authors contributed equally to this work.

reaction (SLER),[47,49–51] of the pore size of the ZIF-8 sheath. The combination of a solvothermal reaction and SLER could realize the formation of thickness-controlled continuous multi-layers of MOF thin films (nanometer scale) on complicated surfaces. The ZIF-8-DMBIM obtained was much more rigid and possesses a smaller aperture than the original ZIF-8 sheath, which promotes the selective penetration of acetone because of its smaller D_k. As a result, the material obtained exhibited the highest selective detection of acetone in the presence of benzene to date.

Results and discussion

The preparation process is shown in Fig. 1 (for further details see the Experimental section). The ZnO nanowire arrays (NWA) were prepared using a typical seed assisted hydrothermal method which had been reported previously.[14,52] Then, Au nanoparticles were deposited onto the surfaces of ZnO NWs to obtain Au–ZnO using the reduction of chloroauric acid ($HAuCl_4$) by sodium borohydride ($NaBH_4$) in aqueous solution. The Au–ZnO not only acted as a gas sensitive core, but was also the sacrificial template to both supply Zn^{2+} for constructing MOF and provide the growth sites for MOF thin films on its surface. After that, the prepared Au–ZnO NWA was immersed into methanol (MeOH) solution containing 2-MIM at 60 °C to grow hydrophobic ZIF-8 thin film not only to suppress the interference of humidity but it can also be used as the matrix MOF for subsequent ligand exchange. The Au–ZnO with a coating of 5 nm, 30 nm or 50 nm thick ZIF-8 thin films were obtained and denoted as Au–ZnO@ZIF 5 nm, Au–ZnO@ZIF 30 nm and Au–ZnO@ZIF 50 nm, respectively. Next, the 2-MIM ligand in the ZIF-8 sheath was exchanged with DMBIM by immersing the Au–ZnO@ZIF into 16 ml of MeOH containing DMBIM and triethylamine (TEA) at 60 °C for 15 h, to obtain Au–ZnO@ZIF-DMBIM.[47,53]

The proton nuclear magnetic resonance (^{1}H-NMR) spectra were used to monitor the model reaction between ZIF-8 crystallite and DMBIM. The ligand exchange molar ratios [$M_{DMBIM}/(M_{DMBIM} + M_{2\text{-}MIM}) \times 100\%$] were calculated by integrating the ^{1}H-NMR signals and it was found that the exchange reaction finished after 10 h (Fig. 2a, for details see the Methods section). Based on the previous results, Au–ZnO@ZIF materials were soaked in MeOH solution containing DMBIM and TEA at 60 °C for 15 h to obtain Au–ZnO@ZIF 5 nm-DMBIM, Au–ZnO@ZIF 30 nm-DMBIM and Au–ZnO@ZIF 50 nm-DMBIM. The ^{1}H-NMR and Fourier-transform infrared (FTIR) spectra confirmed the formation of the ZIF-DMBIM sheath (Fig. 2b, c, S1 and S2, ESI†). The ligand exchange molar ratios [$M_{DMBIM}/(M_{DMBIM} + M_{2\text{-}MIM}) \times 100\%$] were 17.0%, 9.9% and 9.9% for Au–ZnO@ZIF 5 nm-DMBIM, Au–ZnO@ZIF 30 nm-DMBIM and Au–ZnO@ZIF 50 nm-DMBIM, respectively [Fig. 2c and S2 (ESI†)].

In the crystal structure of ZIF-8, the 2-MIM ligand coordinates with Zn^{2+} to form spherical cavities which were further connected with each other to form a three-dimensional porous structure.[54,55] The 2-MIM ligand with a length of ~3.6 Å was partially replaced by DMBIM with a longer length of ~6.0 Åwas mentioned previously (Fig. 1). Compared with ZIF-8, ZIF-8-DMBIM has a significantly narrowed aperture for optimizing the selective adsorption of the molecules with smaller D_k. The ZIF-8-DMBIM has a similar Brunauer–Emmett–Teller surface area and average pore size distribution with those of ZIF-8 when determined using nitrogen (N_2) which has smaller D_k values (Fig. S3, ESI†). However, the absorption capacity of ZIF-8-DMBIM towards acetone (D_k = 0.47 nm), toluene (D_k = 0.585 nm), and ethylbenzene (D_k = 0.60 nm) were ~16%, 23% and 44% lower than those of ZIF-8, respectively (Fig. 2d, S4 and Table S1, ESI†).[47,56] From the acetone and water vapor sorption measurements, it can be seen that the ZIF-8-DMBIM had inherited the excellent hydrophobic properties of ZIF-8 (Fig. S5, ESI†).

Fig. 3a–d show the plane views of Au–ZnO, Au–ZnO@ZIF 5 nm, Au–ZnO@ZIF 30 nm and Au–ZnO@ZIF 50 nm. All of them were NWA structures, where the diameter of the individual nanowire became larger and larger as the thickness of the ZIF-8

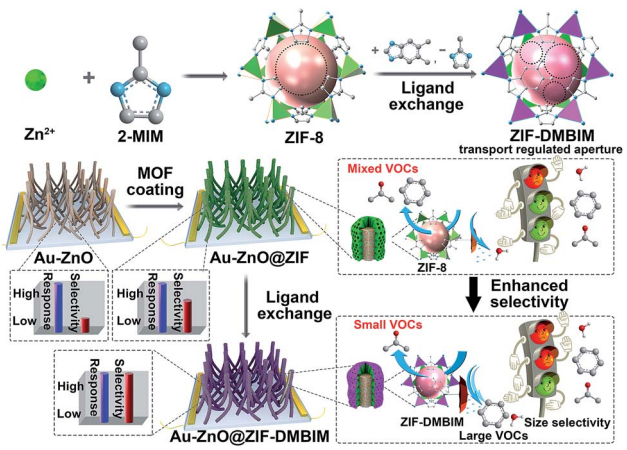

Fig. 1 Schematic illustration of the preparation of Au–ZnO@MOF.

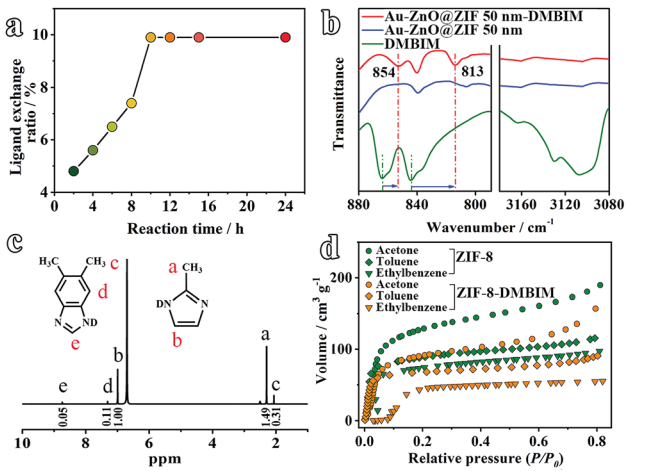

Fig. 2 (a) Time-dependent ligand exchange molar ratio of ZIF-8-DMBIM; (b) FTIR spectra of the DMBIM ligand, Au–ZnO@ZIF 50 nm and Au–ZnO@ZIF 50 nm-DMBIM; (c) ^{1}H-NMR spectra of the digested Au–ZnO@ZIF 50 nm-DMBIM; (d) vapor sorption isotherms of ZIF-8 and ZIF-8-DMBIM.

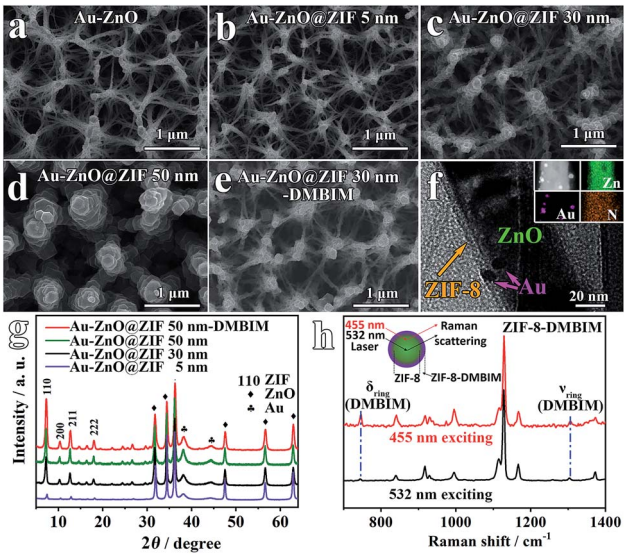

Fig. 3 SEM images of (a) Au–ZnO, (b) Au–ZnO@ZIF 5 nm, (c) Au–ZnO@ZIF 30 nm, (d) Au–ZnO@ZIF 50 nm, and (e) Au–ZnO@ZIF 30 nm-DMBIM, (f) TEM image and EDS mapping images of Au–ZnO@ZIF 5 nm, (g) PXRD patterns of Au–ZnO@MOF NWAs grown on sapphire substrates, (h) Raman spectra of ZIF-8-DMBIM obtained with different laser excitation wavelengths.

sheath increased. As shown in Fig. 3e and S6 (ESI†), after the exchange of ligand, the resultant materials maintained their original morphologies. The transmission electron microscopy (TEM) image of Au–ZnO@ZIF 5 nm shown in Fig. 3f confirms the uniform and continuous coating of the MOF sheath on the Au decorated ZnO nanowires. The corresponding elemental energy dispersive spectrometry (EDS) mapping images (insets of Fig. 3f) of Au, N and Zn, clearly show the ZnO nanowire core with diameter of ~60 nm, Au nanocrystals with diameter of 5–10 nm, and a MOF sheath with a thickness of ~5 nm. The XPS measurements (Fig. S7, ESI†) show that the valence of Au and Zn were 0 and +2, respectively, which were consistent with these of reported Au nanoparticle, ZnO nanowire and ZIF-8.[14,57] Similar results were found for the materials with a thicker MOF sheath (Fig. S8, ESI†). The powder X-ray diffraction (PXRD) patterns of the as prepared MOF coated Au–ZnO NWs were assigned to ZIF-8, ZnO and the Au nanoparticle (Fig. 3g). The PXRD results also revealed the retained crystal structure of the MOF sheath before and after ligand exchange. Compared with the results obtained using a 532 nm laser, the pattern in ultraviolet-visible Raman spectroscopy obtained at 455 nm, which has a shallower penetration depth at the same position of the sample, shows a strong signal of DMBIM (Fig. 3h).[47,58] This result suggested that DMBIM has a higher concentration at the outer surface to form a ZIF-8 topological structure but with smaller apertures.

Materials prepared on sapphire substrates with Ag electrodes were used for sensing tests. The experiments were carried out by placing the previous setup in a sealed and thermostatic quartz chamber. The resistance change of the sensing materials towards different atmospheres was collected as the output signal (for further details see the Methods section). Fig. 4a and S9–S11 (ESI†) show that all of the materials possess the typical behavior of an n-type semiconductor and show an acetone concentration dependent response. The linear response–concentration log–log plots of these materials revealed their similar limit of detection (LOD) in the range of ~0.0001–0.0047 ppm (Fig. S12 and Table S2, ESI†), which was good enough to detect trace levels of acetone. These materials also had similar response and recovery speeds with the values from 3 min to 1 min (Fig. S13–S15, ESI†). The previous results indicated that the MOF sheath with a thickness less than 30 nm had almost no influence on the response of the Au–ZnO nanowire core. However, when the thickness of the MOF sheaths increased to 50 nm, a remarkable decrease of the response and a slower speed was be observed because of: (1) too much ZnO was scarified during the growing of the MOF sheath, which destroyed the Au–ZnO structure (Fig. S8b, ESI†), and (2) the elongated gas transport distance in the MOF layer.

Interestingly, the selectivity of Au–ZnO was significantly enhanced after MOF coating. Humidity strongly interferes with the detection of acetone because of its high concentration in air. After coating with a 5 nm ZIF-8 sheath, the coefficient of variation (CV) of the Au–ZnO decreased from 33% to 16% when the relative humidity (RH) was varied from 0% to 90% (Fig. S11 and S16, ESI†). By increasing the ZIF-8 sheath to 30 nm, the CV was further suppressed to ~6%, thus, indicating excellent anti-humidity interference properties. Furthermore, the Au–ZnO@ZIF 30 nm-DMBIM exhibited much better long-term stability (over four of months testing) of anti-humidity (CV < 5%) than Au–ZnO@ZIF 30 nm (CV > 20%, Fig. S16, ESI†).

One of the more challenging tasks was how to enhance the selectivity of the MOs towards molecules with similar sensing reactivity. As shown in Fig. S17 (ESI†), the Au–ZnO had a broad

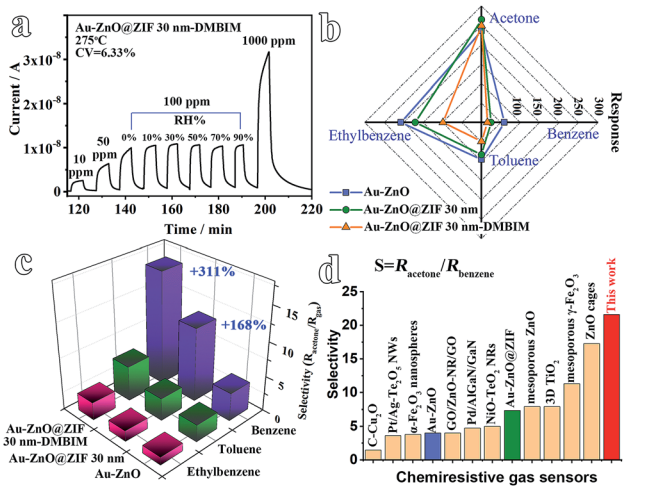

Fig. 4 (a) Response–recovery curves of Au–ZnO@ZIF 30 nm-DMBIM with different concentrations in dry air and up to 100 ppm of acetone with different RH; (b) response comparison of the sensors towards different gases; (c) selectivity comparison of acetone towards three types of benzene; and (d) selectivity comparison with different sensing materials.

response to various gases. However, its response to benzene series gases and ketones was distinctively higher than to other gases. Compared with the benzene series, acetone has a smaller D_k. Fig. 4b shows the response comparison of Au–ZnO, Au–ZnO@ZIF 30 nm and Au–ZnO@ZIF 30 nm-DMBIM towards acetone and three typical members of the benzene series. It was observed that the MOF coating on Au–ZnO optimized its selectivity, followed by the exchange of ligands which remarkably enhanced this performance further. Notably, after coating with ZIF-8 and DMBIM exchange, the prepared materials showed almost no change in response towards acetone. However, the ZIF-8 coating suppressed the response of Au–ZnO to the benzene series. After tuning the aperture of ZIF-8 to a smaller size using ligand exchange, the responses of the material to the benzene series were further depressed. As a result, the selectivity of acetone towards the benzene series ($S = R_{acetone}/R_{benzene\ series}$) for Au–ZnO@ZIF 30 nm-DMBIM achieved improvements of 311.0% for benzene, 115.3% for toluene and 78.5% for ethylbenzene (Fig. 4c and Table S3, ESI†). Even better selectivity improvements of acetone towards the benzene series (440.0% for benzene, 219.0% for toluene and 226.3% for ethylbenzene) were obtained using a thinner MOF sheath (Fig. S18 and S19, ESI†) because of the higher ratio of ligand exchange in Au–ZnO@ZIF 5 nm-DMBIM. As shown in Fig. 4d, compared with the reported materials, Au–ZnO@ZIF 5 nm-DMBIM showed the highest selectivity of acetone to benzene.[59–68] The sensitivity of Au–ZnO@ZIF 5 nm-DMBIM to 100 ppm acetone was ~231, which was comparable with results of previously reported research (Table S4, ESI†).

Linear discriminant analysis (LDA) was used to statistically analyze the sensing data obtained above (for further details see the ESI†).[69,70] The results of the LDA are shown in Table S5 and Fig. S20 (ESI†), demonstrating a 92.0%, 96.1% and 97.2% accuracy of Au–ZnO, Au–ZnO@ZIF 30 nm, and Au–ZnO@ZIF 30 nm-DMBIM, respectively, in classifying 90 trials with a small standard deviation. This analysis showed that coating a layer of MOF sheath and further narrowing its pore size using ligand exchange can remarkably improve the capability of the sensors to distinguish acetone from interfering gases with a high degree of confidence.[69] Notably, compared with other sensing materials, such as carbon nanotubes, MO@MOF can achieve highly accurate discrimination but with fewer devices.[71,72]

Conclusions

In summary, for the first time, it was proposed that the selectivity of a MO chemiresistive sensing material towards molecules that possess similar sensing reactivity can be significantly improved by constructing a MO@MOF core–sheath NWA and modulating the channel traffic of these molecules in the MOF sheath. To demonstrate this, the channel traffic control of acetone and members of the benzene series, which have a similar sensing activity was realized using an *in situ* post-synthetic modification of the pore size of the MOF sheath. The prepared MO@MOF showed the highest selectivity in distinguishing acetone and benzene in all the reported chemiresistive materials. Furthermore, the prepared material also showed very high sensitivity (LOD < 0.1 ppb), fast response and recovery, and excellent long-term stability (CV of ~6% and >4 months) under various humidity (0–90 RH%) conditions. These results should give great inspiration for the design and preparation of high-performance sensing materials and to fulfil the precise detection requirements in breath analysis, intelligent traffic systems, public security affairs, and so on.

Experimental

All the reagents used were purchased commercially and used without further purification.

Preparation of ZnO nanowire arrays

The ZnO NWAs were obtained using a hydrothermal method which was reported previously. Prior to the experiment, the sapphire substrate ($8 \times 10 \times 1$ mm^3, Jing'an Optoelectronics Co., Ltd., China) was washed ultrasonically using deionized water, acetone and ethanol for 10 min before framing the electrodes using Ag paste (SA-5121Q, Wuhan Youle Optoelectronics Technology Co., Ltd., China) and Au wires. A layer of zinc acetate sprayed on the surface of sapphire substrate was calcined at 350 °C for 0.5 h to first form the ZnO seed. Then the substrate was dipped upside down into a mixture of an aqueous solution of 8 ml of 0.02 M zinc acetate dihydrate ($ZnAc_2 \cdot 2H_2O$) and 8 ml of 0.02 M hexamethylenetetramine in a sealed autoclave with a stainless steel shell at 95 °C for 16 h inside an oven. Subsequently, the substrate was removed and washed three times with deionized water and then heated at 550 °C for 2 h.

Preparation of Au–ZnO nanowire array

To prepare the Au–ZnO NWA, 0.5 ml of 0.02 M sodium citrate, 0.2 ml of 25.4 mM chloroauric acid ($HAuCl_4 \cdot 4H_2O$) and 0.6 ml 0.095 M of $NaBH_4$ aqueous solutions were sequentially added into 39 ml of deionized water under continuous stirring at room temperature. Then the previously prepared ZnO NWAs were rapidly immersed into this mixture solution and stirred for 30 min. After that, the substrate was washed with deionized water and dried in a vacuum drying oven at room temperature for further use.

Preparation of Au–ZnO@ZIF nanowire arrays

The Au–ZnO@ZIF NWAs were prepared using the following procedure: the Au–ZnO NWAs were dipped in 0.5 M of a methanolic solution of 2-MIM for different times to form a ZIF-8 sheath layer thin film at 60 °C. Then the substrates were rinsed with MeOH and dried in a stream of nitrogen. In order to obtain ZIF-8 with different thickness on the surface of Au–ZnO, the reaction times were controlled to 3 h, 12 h and 24 h. The samples were labeled Au–ZnO@ZIF 5 nm, Au–ZnO@ZIF30 nm and Au–ZnO@ZIF50 nm.

Preparation of Au–ZnO@ZIF-DMBIM nanowire arrays

The Au–ZnO@ZIF NWAs were dipped upside down into 16 ml of MeOH in a Teflon-lined stainless steel autoclave containing

0.08 g of DMBIM (0.034 M) and 0.08 ml of TEA. After heating at 60 °C for 15 h, the product was washed with MeOH and then stored for later use.

Preparation of ZIF-8-DMBIM nanoparticles

A SLER method was used to prepare ZIF-8-DMBIM nanoparticles. The DMBIM, MeOH, TEA and fresh ZIF-8 (preparation method as reported in the literature[73]) nanocrystals were dispersed in MeOH in a Teflon-lined stainless steel autoclave (weight composition: ZIF-8–DMBIM–TEA–MeOH = 1 : 1 : 0.7 : 160). After heated at 60 °C for 15 h, the product was centrifuged and washed with three times with MeOH and then stored for later use.

Characterization

Infrared spectra were recorded using a Nicolet 6700 FTIR-attenuated total reflectance (ATR) spectrophotometer. The XRD analyses were carried out using a Rigaku MiniFlex600 X-ray diffractometer with a one-dimensional array detector using CuKα radiation (λ = 1.54178 Å). The ^{1}H-NMR spectra were acquired using a Bruker AVANCE III 400 MHz (SB) spectrometer at room temperature. A solution of 35 wt% deuterium chloride (DCl) was used to dissolve the nanoparticles and deuterium dimethylsulfoxide (DMSO-d6) was used as solvent. The morphology of both virgin ZnO and composite ZnO@Au@ZIF-8-DMBIM NWAs were studied using a Jeol JSM-6700F scanning electron microscope (SEM) and a Tecnai F20 TEM. The surface chemical analysis was investigated using X-ray photoelectron spectroscopy (XPS) on a ThermoScientific ESCALAB 250Xi XPS system. For the acetone and water adsorption spectra, the samples were activated at 200 °C for 6 h before measurement using a Hiden IGA-100B Intelligent Gravimetric Sorption Analyser at 25 °C. The thermogravimetry (TG) was carried out using a Netzsch STA 449 C analyzer with a heating rate of 10 °C min^{-1} in flowing ambient air. The volatile organic compounds (VOCs) and water adsorption were measured using the Hiden IGA-100B Intelligent Gravimetric Sorption Analyser at 25 °C.

Gas sensor characterization

All the samples were activated at 275 °C for 4 h in a dry air atmosphere (21% O_2 and 79% N_2) before testing. The gas sensing performance was examined using a home-made system as reported previously.[14] The target gas (Beijing Hua Yuan Gas Chemical Industry Co., Ltd., China) concentrations were controlled by changing the mixing ratio of dry air and dry air-balanced analyte gas using CS200C mass flow controllers (Beijing Sevenstar Qualiflow Electronic Equipment Manufacturing Co., Ltd., China). The constant flow was 600 ml min^{-1}, the current was recorded using a Keithley 2602B SourceMeter with a 5 V bias on sensor. It took ~0.65 min to fully fill the quartz chamber when the gas flow was 600 ml min^{-1}. The CV was calculated using $R_{SD}/R_{average} \times 100\%$, R_{SD} and $R_{average}$ are the standard deviation (SD) and average value of the responses.

According to the conductance model, which was limited by the electron transport across the intergranular Schottky barrier, the response equation of grain-based gas sensors, was obtained as the following equation (for resistance increase):

$$\log(R_{gas}/R_{air} - 1) = \log A_g + \beta \log p_g \quad (1)$$

where p_g is the gas partial pressure, A_g is a prefactor, and the exponent β is the response order.

Conflicts of interest

There are no conflicts to declare.

Acknowledgements

This work was supported by National Key R&D Program of China (2017YFA0206802), the Natural Science Foundation (NSF) of China (21822109, 21801243, 21805276, 21773245, 21850410462, 51602311), the Strategic Priority Research Program of Chinese Academy of Sciences (CAS) (XDB20000000), the Key Research Program of Frontier Science, CAS (QYZDB-SSW-SLH023), and the NSF of Fujian Province (2017J05094, 2019J01129), the Youth Innovation Promotion Association of CAS, and the International Partnership Program of CAS (121835KYSB201800). The Authors wish to thank Prof. Li-Min Zheng and Prof. Song-Song Bao from Nanjing University for their kind support and help with the in gas sorption measurements.

References

1 J. Zhang, X. Liu, G. Neri and N. Pinna, *Adv. Mater.*, 2016, **28**, 795–831.
2 W. Hu, L. Wan, Y. Jian, C. Ren, K. Jin, X. Su, X. Bai, H. Haick, M. Yao and W. Wu, *Adv. Mater. Technol.*, 2019, **4**, 1800488.
3 H. Haick, Y. Y. Broza, P. Mochalski, V. Ruzsanyi and A. Amann, *Chem. Soc. Rev.*, 2014, **43**, 1423–1449.
4 M. Phillips, R. N. Cataneo, A. R. Cummin, A. J. Gagliardi, K. Gleeson, J. Greenberg, R. A. Maxfield and W. N. Rom, *Chest*, 2003, **123**, 2115–2123.
5 R. Yazbeck, S. E. Jaenisch and D. I. Watson, *World J. Gastroenterol.*, 2016, **22**, 10077.
6 H.-J. Kim and J.-H. Lee, *Sens. Actuators, B*, 2014, **192**, 607–627.
7 K. Suematsu, W. Harano, T. Oyama, Y. Shin, K. Watanabe and K. Shimanoe, *Anal. Chem.*, 2018, **90**, 11219–11223.
8 H.-J. Lin, H. Gao and P.-X. Gao, *Appl. Phys. Lett.*, 2017, **110**, 043101.
9 Z. Meng, R. M. Stolz, L. Mendecki and K. A. Mirica, *Chem. Rev.*, 2019, **119**, 478–598.
10 T. Ueda, T. Maeda, Z. Huang, K. Higuchi, K. Izawa, K. Kamada, T. Hyodo and Y. Shimizu, *Sens. Actuators, B*, 2018, **273**, 826–833.
11 L. Zhang, P. Cui, H. Yang, J. Chen, F. Xiao, Y. Guo, Y. Liu, W. Zhang, F. Huo and B. Liu, *Adv. Sci.*, 2016, **3**, 1500243.
12 M. Zhao, K. Yuan, W. Yun, G. Li, J. Guo, G. Lin, W. Hu, H. Zhao and Z. Tang, *Nature*, 2016, **539**, 76.

13 G. Lal, M. Derakhshandeh, F. Akhtar, D. M. Spasyuk, J.-B. Lin, M. Trifkovic and G. K. Shimizu, *J. Am. Chem. Soc.*, 2018, **141**, 1045–1053.
14 M. S. Yao, W. X. Tang, G. E. Wang, B. Nath and G. Xu, *Adv. Mater.*, 2016, **28**, 5229–5234.
15 K. Otsubo, T. Haraguchi and H. Kitagawa, *Coord. Chem. Rev.*, 2017, **346**, 123–138.
16 L. Jiao, G. Wan, R. Zhang, H. Zhou, S. H. Yu and H. L. Jiang, *Angew. Chem., Int. Ed.*, 2018, **57**, 8525–8529.
17 Y. Y. Zhu, G. Lan, Y. Fan, S. S. Veroneau, Y. Song, D. Micheroni and W. Lin, *Angew. Chem., Int. Ed.*, 2018, **57**, 14090–14094.
18 N. C. Burtch, J. Heinen, T. D. Bennett, D. Dubbeldam and M. D. Allendorf, *Adv. Mater.*, 2018, **30**, 1704124.
19 S. Bhattacharya, W. W. Ayass, D. H. Taffa, A. Schneemann, A. L. Semrau, S. Wannapaiboon, P. J. Altmann, A. Pöthig, T. Nisar, T. Balster, N. C. Burtch, V. Wagner, R. A. Fischer, M. Wark and U. Kortz, *J. Am. Chem. Soc.*, 2019, **141**, 3385–3389.
20 J. Liu, J. Ye, Z. Li, K.-i. Otake, Y. Liao, A. W. Peters, H. Noh, D. G. Truhlar, L. Gagliardi, C. J. Cramer, O. K. Farha and J. T. Hupp, *J. Am. Chem. Soc.*, 2018, **140**, 11174–11178.
21 H. Wang, P. Rassu, X. Wang, H. Li, X. Wang, X. Wang, X. Feng, A. Yin, P. Li, X. Jin, S. L. Chen, X. Ma and B. Wang, *Angew. Chem., Int. Ed.*, 2018, **57**, 16416–16420.
22 L. Heinke and C. Wöll, *Adv. Mater.*, 2019, **31**(26), 1806324.
23 C. Cao, D. D. Ma, Q. Xu, X. T. Wu and Q. L. Zhu, *Adv. Funct. Mater.*, 2019, **29**, 1970033.
24 J. Baek, B. Rungtaweevoranit, X. Pei, M. Park, S. C. Fakra, Y.-S. Liu, R. Matheu, S. A. Alshmimri, S. Alshehri, C. A. Trickett, G. A. Somorjai and O. M. Yaghi, *J. Am. Chem. Soc.*, 2018, **140**, 18208–18216.
25 J. Pang, S. Yuan, J.-S. Qin, C. T. Lollar, N. Huang, J. Li, Q. Wang, M. Wu, D. Yuan, M. Hong and H.-C. Zhou, *J. Am. Chem. Soc.*, 2019, **141**, 3129–3136.
26 M. S. Denny, L. R. Parent, J. P. Patterson, S. K. Meena, H. Pham, P. Abellan, Q. M. Ramasse, F. Paesani, N. C. Gianneschi and S. M. Cohen, *J. Am. Chem. Soc.*, 2018, **140**, 1348–1357.
27 C. Gu, N. Hosono, J.-J. Zheng, Y. Sato, S. Kusaka, S. Sakaki and S. Kitagawa, *Science*, 2019, **363**, 387–391.
28 P.-Q. Liao, N.-Y. Huang, W.-X. Zhang, J.-P. Zhang and X.-M. Chen, *Science*, 2017, **356**, 1193–1196.
29 H. Tian, H. Fan, M. Li and L. Ma, *ACS Sens.*, 2016, **1**, 243–250.
30 J. Dechnik, J. Gascon, C. J. Doonan, C. Janiak and C. J. Sumby, *Angew. Chem., Int. Ed.*, 2017, **56**, 9292–9310.
31 K. Adil, Y. Belmabkhout, R. S. Pillai, A. Cadiau, P. M. Bhatt, A. H. Assen, G. Maurin and M. Eddaoudi, *Chem. Soc. Rev.*, 2017, **46**, 3402–3430.
32 X.-L. Liu, Y.-S. Li, G.-Q. Zhu, Y.-J. Ban, L.-Y. Xu and W.-S. Yang, *Angew. Chem., Int. Ed.*, 2011, **50**, 10636–10639.
33 L. Li, R.-B. Lin, R. Krishna, H. Li, S. Xiang, H. Wu, J. Li, W. Zhou and B. Chen, *Science*, 2018, **362**, 443–446.
34 A. C. Forse, P. J. Milner, J.-H. Lee, H. N. Redfearn, J. Oktawiec, R. L. Siegelman, J. D. Martell, B. Dinakar, L. B. Porter-Zasada and M. I. Gonzalez, *J. Am. Chem. Soc.*, 2018, **140**, 18016–18031.
35 M. G. Campbell, D. Sheberla, S. F. Liu, T. M. Swager and M. Dincă, *Angew. Chem., Int. Ed.*, 2015, **127**, 4423–4426.
36 M.-S. Yao, X.-J. Lv, Z.-H. Fu, W.-H. Li, W.-H. Deng, G.-D. Wu and G. Xu, *Angew. Chem., Int. Ed.*, 2017, **56**, 16510–16514.
37 Y. V. Kaneti, S. Dutta, M. S. A. Hossain, M. J. A. Shiddiky, K.-L. Tung, F.-K. Shieh, C.-K. Tsung, K. C.-W. Wu and Y. Yamauchi, *Adv. Mater.*, 2017, **29**, 1700213.
38 C. V. Nguyen, Y.-T. Liao, T.-C. Kang, J. E. Chen, T. Yoshikawa, Y. Nakasaka, T. Masuda and K. C. W. Wu, *Green Chem.*, 2016, **18**, 5957–5961.
39 F.-K. Shieh, S.-C. Wang, C.-I. Yen, C.-C. Wu, S. Dutta, L.-Y. Chou, J. V. Morabito, P. Hu, M.-H. Hsu, K. C. W. Wu and C.-K. Tsung, *J. Am. Chem. Soc.*, 2015, **137**, 4276–4279.
40 C. Wang, J. Kim, M. Kim, H. Lim, M. Zhang, J. You, J.-H. Yun, Y. Bando, J. Li and Y. Yamauchi, *J. Mater. Chem. A*, 2019, **7**, 13743–13750.
41 Z.-X. Cai, Z.-L. Wang, J. Kim and Y. Yamauchi, *Adv. Mater.*, 2019, **31**, 1804903.
42 Q. Yang, C. C. Yang, C. H. Lin and H. L. Jiang, *Angew. Chem., Int. Ed.*, 2019, **58**, 3511–3515.
43 D. Zhao, C. Kong, H. Du, Y. Yan, Z. U. Wang, H.-L. Jiang and L. Chen, *Sci. China Mater.*, 2019, **62**, 448–454.
44 Y. Li, Z. Yang, Y. Wang, Z. Bai, T. Zheng, X. Dai, S. Liu, D. Gui, W. Liu and M. Chen, *Nat. Commun.*, 2017, **8**, 1354.
45 Z. Xiao, J. Meng, Q. Li, X. Wang, M. Huang, Z. Liu, C. Han and L. Mai, *Sci. Bull.*, 2018, **63**, 46–53.
46 Y. Wu, H. Pang, W. Yao, X. Wang, S. Yu, Z. Yu and X. Wang, *Sci. Bull.*, 2018, **63**, 831–839.
47 X. Liu, Y. Li, Y. Ban, Y. Peng, H. Jin, H. Bux, L. Xu, J. Caro and W. Yang, *Chem. Commun.*, 2013, **49**, 9140–9142.
48 T. Islamoglu, S. Goswami, Z. Li, A. J. Howarth, O. K. Farha and J. T. Hupp, *Acc. Chem. Res.*, 2017, **50**, 805–813.
49 O. Karagiaridi, M. B. Lalonde, W. Bury, A. A. Sarjeant, O. K. Farha and J. T. Hupp, *J. Am. Chem. Soc.*, 2012, **134**, 18790–18796.
50 M. Kondo, S. Furukawa, K. Hirai and S. Kitagawa, *Angew. Chem., Int. Ed.*, 2010, **49**, 5327–5330.
51 B. J. Burnett, P. M. Barron, C. Hu and W. Choe, *J. Am. Chem. Soc.*, 2011, **133**, 9984.
52 L. E. Greene, M. Law, D. H. Tan, M. Montano, J. Goldberger, G. Somorjai and P. Yang, *Nano Lett.*, 2005, **5**, 1231–1236.
53 K. Eum, K. C. Jayachandrababu, F. Rashidi, K. Zhang, J. Leisen, S. Graham, R. P. Lively, R. R. Chance, D. S. Sholl, C. W. Jones and S. Nair, *J. Am. Chem. Soc.*, 2015, **137**, 4191–4197.
54 K. S. Park, Z. Ni, A. P. Côté, J. Y. Choi, R. Huang, F. J. Uribe-Romo, H. K. Chae, M. O'Keeffe and O. M. Yaghi, *Proc. Natl. Acad. Sci. U. S. A.*, 2006, **103**, 10186–10191.
55 X.-C. Huang, Y.-Y. Lin, J.-P. Zhang and X.-M. Chen, *Angew. Chem., Int. Ed.*, 2006, **118**, 1587–1589.
56 K. Zhang, R. P. Lively, C. Zhang, R. R. Chance, W. J. Koros, D. S. Sholl and S. Nair, *J. Phys. Chem. Lett.*, 2013, **4**, 3618–3622.
57 Y. Lu, W. Zhan, Y. He, Y. Wang, X. Kong, Q. Kuang, Z. Xie and L. Zheng, *ACS Appl. Mater. Interfaces*, 2014, **6**, 4186–4195.
58 M. Li, Z. Feng, G. Xiong, P. Ying, Q. Xin and C. Li, *J. Phys. Chem. B*, 2001, **105**, 8107–8111.

59 B. Bhowmik, V. Manjuladevi, R. Gupta and P. Bhattacharyya, *IEEE Sens. J.*, 2016, **16**, 3488–3495.
60 J. He, X. Rao, C. Yang, J. Wang, X. Su and C. Niu, *Sens. Actuators, B*, 2014, **201**, 213–221.
61 Z. Lin, F. Guo, C. Wang, X. Wang, K. Wang and Y. Qu, *RSC Adv.*, 2014, **4**, 5122–5129.
62 S. Park, G.-J. Sun, H. Kheel, C. Lee and K. Kim, *J. Korean Phys. Soc.*, 2015, **67**, 648–653.
63 W. Li, X. Wu, N. Han, J. Chen, X. Qian, Y. Deng, W. Tang and Y. Chen, *Sens. Actuators, B*, 2016, **225**, 158–166.
64 S. Park, G.-J. Sun, H. Kheel, S. Choi and C. Lee, *J. Nanosci. Nanotechnol.*, 2016, **16**, 8589–8593.
65 Z. Xie, N. Han, W. Li, Y. Deng, S. Gong, Y. Wang, X. Wu, Y. Li and Y. Chen, *Phys. Status Solidi A*, 2017, **214**, 1600904.
66 S. Das, S. Ghosh, R. Kumar, A. Bag and D. Biswas, *IEEE Trans. Electron Devices*, 2017, **64**, 4650–4656.
67 P. Wang, X. Zhang, S. Gao, X. Cheng, L. Sui, Y. Xu, X. Zhao, H. Zhao and L. Huo, *Sens. Actuators, B*, 2017, **241**, 967–977.
68 B. A. Vessalli, C. A. Zito, T. M. Perfecto, D. P. Volanti and T. Mazon, *J. Alloys Compd.*, 2017, **696**, 996–1003.
69 M. G. Campbell, S. F. Liu, T. M. Swager and M. Dinca, *J. Am. Chem. Soc.*, 2015, **137**, 13780–13783.
70 P. C. Jurs, G. Bakken and H. McClelland, *Chem. Rev.*, 2000, **100**, 2649–2678.
71 F. Wang and T. M. Swager, *J. Am. Chem. Soc.*, 2011, **133**, 11181–11193.
72 V. Schroeder, S. Savagatrup, M. He, S. Lin and T. M. Swager, *Chem. Rev.*, 2019, **119**, 599–663.
73 J. Cravillon, S. Münzer, S.-J. Lohmeier, A. Feldhoff, K. Huber and M. Wiebcke, *Chem. Mater.*, 2009, **21**, 1410–1412.